arXiv:cond-mat/9306061v1 30 Jun 1993

Bubble Growth in Superfluid ^{3}He: The Dynamics of the Curved A-B Interface

Jens Johannesson*and Mario Liu

Institut für Theoretische Physik, Universität Hannover

D-3000 Hannover 1, F. R. Germany

June 25, 1993

PACS-numbers: 67.57.-z, 67.55.Fa ITP-UH 11/93

Abstract

We study the hydrodynamics of the A-B interface with finite curvature. The interface tension is shown to enhance both the transition velocity and the amplitudes of second sound. In addition, the magnetic signals emitted by the growing bubble are calculated, and the interaction between many growing bubbles is considered.

*e-mail: johan@kastor.itp.uni-hannover.de

1 Introduction

The interface between the A- and B-phase of ^{3}He is the only known boundary between two superfluid systems. The interface motion that accompanies the first order phase transition from the undercooled A- into the B-phase is subject to extended experimental [1 – 4] and theoretical [5 – 9] investigation.

Within the hydrodynamic regime, the structure of the interface dynamics can be rigorously determined by connecting the hydrodynamic modes on both sides of the interface with the appropriate connecting conditions (CoCos). This has already been done [7, 8, 9] for the planar interface. In the present work, we generalize the hydrodynamic description to interfaces of finite curvature, taking as an example spherical B-phase bubbles growing in a bath of undercooled A-phase.

To gain a qualitative understanding, consider first planar growth. For small growth velocities, the released latent heat serves as the source for two second sound step functions, emitted in opposite directions [7]. The steps move with c_{2A} and $-c_{2B}$ if the A-phase is located on the right and c_2 denotes the second sound velocity. If the interface velocity $\dot{u}$ becomes larger than c_2, both steps are left behind in the B-phase. The same is true for spin waves if an external magnetic field produces excess magnetization at the interface [8]. The reference velocity is now of course the spin wave velocity c_s, rather than c_2.

Qualitatively, bubble growth is not much different, except that the surface tension delivers an extra push towards the energetically more favorable B-phase: Neglecting the anisotropy, radial step functions of second sound are emitted out- and inward for $\dot{u} \ll c_2$. The inward moving step functions quickly equalize the temperature distribution within the B-phase bubble. For $\dot{u} \gg c_2$, both radial waves of second sound remain inside the bubble while the temperature remains homogeneous in the A-phase. The spin wave and the magnetization behave accordingly. (Though spin waves are emitted only for higher interface velocities $\dot{u} \gtrsim 1m/s \gg c_2$ [8]) The case $\dot{u} \gg c_\mathrm{s}$ may seem academic but one really cannot discount the possibility that it was indeed already observed [3, 8]. Then, even both spin waves remain inside the bubble where neither the temperature nor the magnetization

is homogeneous. Causality sees to it that the A-phase is completely unperturbed.

The complication of bubble growth is in its time dependence. While planar growth keeps both $\dot{u}$ and the amplitudes of the emitted waves constant, neither are in bubble growth. The growth velocity is not constant because the pushing surface tension, proportional to the inverse of the bubble radius $R(t)$, is not. The amplitudes are not constant, because first of all, they vary as $1/r$ when moving away from the interface; second, the amplitudes in addition are functions of $\dot{R}(t)$. (In fact, there is a retardation effect, the amplitudes are functions of $\dot{R}(t - t_f)$, where t_f is the time of flight $t_f = (r - R)/c_2$ or $(r - R)/c_\mathrm{s}$.)

The anisotropy of c_2 and c_s will distort the radial wave into an elliptical shape, with the principal axes being parallel and perpendicular to $\hat{\ell}$, the orbital preferred direction. (We presume $\hat{\ell}$ to be uniform.) In addition, the growth and Kapitza coefficients are also $\hat{\ell}$-dependent, and this directly distorts the bubble. (Given enough time, of course, the surface tension will drive the bubble into the shape that minimizes the surface energy; generally, it is somewhere inbetween, reflecting some stationary balance between the surface tension and the uneven growth.) Assuming the same eccentricity for both ellipses, we can rescale to obtain isotropic growth and radial waves to perform the calculations. Afterwards, the distortion into elliptical waves is achieved by taking the correct value of the anisotropic velocity for the two principle axes.

If there are many bubbles present, their growth can be considered completely independent for $\dot{R} > c_2$, because the magnetic signals barely feed back to the growth [8], while the second sound waves, which do feed back, are confined to the interior of the bubbles. For $\dot{R} < c_2$ however, the many emitted second sound waves heat up the surrounding A-phase. Since the latent heat is not completely evacuated, the growth velocity slows down accordingly.

A B-phase bubble is thermodynamically stable only if its radius exceeds the critical value $R_c = \alpha/(\rho\,\Delta\mu)$ [5, 11], where α denotes the interface tension and $\Delta\mu = \mu_B - \mu_A$ is the difference in the chemical potential across the interface (for every quantity X, we define: $\langle X\rangle = (X_A + X_B)/2$ and $\Delta X = X_B - X_A$). Since $\Delta\mu$ vanishes at the coexistence point, R_c diverges if T approaches T_{AB}. At lower temperatures, $R_c < l_{QP}$, where l_{QP} is

the mean free path of the quasi particles, the hydrodynamic description becomes valid only after the bubble has nucleated and reached an appropriate size by ballistic processes. Fig. 1 shows the respective length scales as a function of temperature. As pointed out by Leggett and Yip [5] the nucleation process itself is likely to be of exotic nature.

The CoCos [7, 8, 9], we shall employ fall into three categories, those for the conserved quantities, those for the symmetry variables and the parameterization of the surface entropy production. For the locally conserved quantities, the CoCos state the continuity of the respective currents, expressing the fact that conserved quantities cannot accumulate within, or be depleted from, a region of microscopic width. This is not true, however, if the momentum current traverses a curved interface, where the radial bulk momentum current differs by the interfacial momentum current [11] α/R. (Note that $\alpha < 0$: In equilibrium the pressure is larger on the A-phase side.) With prime denoting the rest frame of the interface, the CoCos are:

$$\Delta g' = 0, \tag{1}$$

$$\Delta(p + \Pi') = \frac{\alpha}{R}, \tag{2}$$

$$\Delta Q' = 0, \tag{3}$$

$$\Delta \mathbf{j}^{\mathrm{spin}} = 0. \tag{4}$$

The notations: mass current g', pressure p, nonlinear part of the momentum current Π', energy current Q' and spin current $\mathbf{j}^{\mathrm{spin}}$.

The behavior of the symmetry variables in the interface region is related to the elasticity of the order parameter within the interface. Since the elastic coefficients are of comparable order of magnitude in the interface as in the bulk liquid, we have coherence of the symmetry variables across the interface. More specifically, we have for the phase angle ϕ and the rotation angle $\vec{\Theta}$ in spin space

$$\Delta\, \phi = 0, \tag{5}$$

$$\Delta\, \vec{\Theta} = 0. \tag{6}$$

It is by means of Eq. (5) that the interface tension acts in accelerating the growth process.

Since (5) implies $\Delta\mu = 0$, the interface tension couples to the dynamics through the pressure dependency of the chemical potential and CoCo (2) is implicitly incorporated. When the growth starts at $R = R_c$ we find the initial interface velocity to be twice as fast as in the planar case. This effect should be accessible to experimental probe.

The irreversibility of the phase transition is accounted for by the growth coefficient K for $\dot{u} \gg c_2$, and by the Kapitza resistance κ for $\dot{u} \ll c_2$, respectively. Both K and κ are effective, integrated quantities and functions of various surface Onsager coefficients, thermodynamic susceptibilities and bulk transport coefficients [9]. The rate of interface entropy production $R_S = -\langle T \rangle \, \Delta \, f'$ is then respectively given as

$$R_S = \frac{g'^2}{K} \qquad \text{or} \qquad R_S = \frac{\langle f' \rangle^2}{\kappa}, \tag{7}$$

where f' is the entropy current. So except Eq. (2), all CoCos retain their form of planar growth.

The solution of these CoCos in Sec. 3 shows the following result: The growth velocity decreases with $1/R$ towards the limiting value $\dot{R}_\infty$ (of the planar growth); while the amplitudes of second sound generated during the growth show some intricate time dependency.

In Sec. 2, we discuss the magnetic signals emitted by the growing bubble. These are more accessible to experimental probe.

The general case of N interacting bubbles V is discussed in Sec. 4.

2 Spin waves

We consider the magnetic signals emitted during bubble growth for $\dot{R} \ll c_\mathrm{s}$. As discussed in Ref. [8], the magnetization is for $\dot{R} \lesssim (H/\mathrm{kOe})^{-1}\,\mathrm{m/s}$ essentially given by its equilibrium values $\chi_{A,B}\, H$. The small deviations from the equilibrium values do not change much, going from planar to bubble growth. For higher velocities, $\dot{R} \gtrsim 1\,\mathrm{m/s}$, the dipole-interaction is negligible, the magnetic signals turn into spin waves and become delocalized. Here, the circumstances of bubble growth are more complicated and are what we shall consider.

2.1 Interface dynamics

The feed-back of the spin-dynamics to the growth velocity $\dot{R}$ is negligible if $\dot{R}$ is not too close to $c_{\mathrm{s}A}$ [8]. Hence, we may take $\dot{R}$, as calculated in Sec. 3 without the inclusion of the magnetic fields, as an input:

$$\dot{R} = \dot{R}_\infty \left(1 + \frac{R_c}{R}\right), \tag{8}$$

where $\dot{R}_\infty$ denotes the limiting value of the interface velocity for large R, i.e. $\dot{R}_\infty = \dot{u}$ of planar growth. The explicit values for $\dot{R}_\infty$ are given in Eqs. (27) and (39) for weak and strong undercooling, respectively. The solution of the differential equation (8) subject to the initial condition $R(t=0) = R_0$ then reads

$$t\,\dot{R}_\infty = R - R_0 + R_c \ln\left(\frac{R_0 + R_c}{R + R_c}\right). \tag{9}$$

The inverse of (9) can also be written in a closed form, see App. A.

2.2 Spin-Hydrodynamics

We shall work with the longitudinal model [8], which contains only two dynamical variables: the magnetization and the dipole angle Θ (where Θ_A is that between $\hat{d}$ and $\hat{\ell}$, and Θ_B is the angle around $\hat{n}$).

The initial scenario contains a B-phase bubble of radius R_0, exposed to a homogeneous magnetic field $\vec{H}$. Within the bubble, we assume a uniform $\hat{n}$-texture, parallel to $\vec{H}$; in the surrounding A-phase we have $\hat{d} \perp \vec{H}$, $\hat{\ell} \parallel \hat{d}$. Although the uniformity of the $\hat{n}$-texture contradicts the equilibrium A-B interface [12], we shall neglect this complication as in Ref. [8].

The coordinates are chosen such that $\vec{H}$ points in the z-direction, while the x-axis coincides with $\hat{\ell}$. The spin-hydrodynamics in the A-phase is then given by the wave equation

$$\ddot{\Theta}_A - c_{\mathrm{s}\parallel}^2 \partial_x^2 \Theta_A - c_{\mathrm{s}\perp}^2 (\partial_y^2 + \partial_z^2)\,\Theta_A = 0, \tag{10}$$

where $c_{\mathrm{s}\parallel}$ and $c_{\mathrm{s}\perp}$ denote the spin wave velocities parallel and perpendicular to the preferred direction $\hat{\ell}$. The consequences of neglecting spin diffusion will be discussed at the end of this section.

Eq. 10 shows that the outgoing wave fronts will be of ellipsoidal shape with a rotational symmetry around $\hat{\ell}$. Assuming a growing bubble with the same eccentricity, as discussed in the introduction, we may distort the coordinates to render both ellipsoids (interface and wave front) spherical:

$$\ddot{\Theta}_A - c_{\mathrm{s}A}^2 \Delta_r \Theta_A = 0, \quad \omega_A = \dot{\Theta}_A, \quad v_A = \partial_r \Theta_A. \tag{11}$$

(v_A is the spin-superfluid velocity.)

The B-phase spindynamics need not be considered explicitly. After the initial time lag of $R_0/c_{\mathrm{s}B}$, the imploding wave front meets at the center. There, the excess magnetization (always parallel to the external field $\vec{H}$) from opposite directions add up, while the spin superfluid velocities $\nabla\,\Theta_B$ (all having the same sign along the radial direction) from opposite directions cancel. So homogeneous magnetization and vanishing $\nabla\,\Theta_B$ is a good approximation.

2.3 Connecting Conditions

With $\dot{R} \ll c_{\mathrm{s}A}$, we can safely neglect terms of order $\dot{R}\,v_A$ and $\dot{R}\,\delta S$; the CoCos (6) and (4) therefore take the simplified form

$$0 = \Delta\omega, \tag{12}$$

$$0 = \gamma H \dot{R} \Delta\chi - \chi_A c_{\mathrm{s}A}^2 v_A, \tag{13}$$

with gyromagnetic ratio γ and susceptibility χ. Working with the longitudinal model, only one of the three relations (6) is needed here.

2.4 Solution of the Connecting Conditions

The procedure to determine the space and time dependency of the radial waves from their CoCos is given below:

In the first step, we calculate the values of the general solution

$$\Theta_A = \frac{f(r - c_{\mathrm{s}A}\,t)}{r} \tag{14}$$

at the interface (subscript I) from the CoCos (12, 13).

Substituting the time dependent bubble radius $R(t)$ for r, we find

$$\omega_A\,|_I \;=\; (\partial_t \Theta_A(r,t))\,|_{r=R(t)} = -c_{\mathrm{s}A}\,\frac{f'(r-c_{\mathrm{s}A}\,t)}{r}\bigg|_{r=R(t)}, \tag{15}$$

$$v_A\,|_I \;=\; (\partial_r \Theta_A(r,t))\,|_{r=R(t)} = \left(\frac{f'(r-c_{\mathrm{s}A}\,t)}{r} - \frac{f(r-c_{\mathrm{s}A}\,t)}{r^2}\right)\bigg|_{r=R(t)}. \tag{16}$$

where f' denotes the derivative of f with respect to its argument. Now, the amplitudes at the interface are functions of time only. For sake of clarity, we introduce an auxiliary function by

$$F(t) = f\left(R(t) - c_{\mathrm{s}A}\,t\right) \equiv f\left(\bar{R}(t)\right), \tag{17}$$

implying

$$f' = \frac{\partial_t F(t)}{\dot{R} - c_{\mathrm{s}A}}. \tag{18}$$

The CoCos (12, 13) thereby turn into differential equations for $F(t)$ which can be solved.

Having obtained $F(t)$ with the appropriate initial condition $F(t=0)=0$, the next step is to reconstruct the (r,t)-dependency of f, where we need the inverse function of $\bar{R}(t)$:

$$F\left(t(\bar{R})\right) = f(\bar{R}). \tag{19}$$

Given $f(\bar{R})$, we can substitute $\bar{R} = r - c_{\mathrm{s}A}\,t$ and obtain ω_A and v_A for all r, t via Eq. (11).

For technical reasons, however, we modify this procedure and eliminate the time t with the inverse of $R(t)$, instead of eliminating r by $R(t)$, as described above. The reader is referred to App. B for the details of the calculation and the result.

For the qualitative features cf. Figs. 2 and 3. The spatial variation of the outgoing radial wave is illustrated for different times. Each curve displays two effects. First the $1/r$-decrease as the wave moves out, and second the amplitude at r,t is a function of $\dot{R}$ at $t = (r-R)/c$, a retardation effect. The line at the upper surface of the box marks the location of the bubble surface, relative to the starting value. Below, one can track the decrease of the amplitudes at the interface. As will be shown in Sec. 3, these plots also visualize the second sound amplitudes, emitted by a slowly growing bubble.

At the head of the shock wave, i.e. where $r = R_0 + c_{sA}\,t$, the expressions for the amplitudes simplify to become

$$v_A(t) = \frac{\gamma H}{c_{sA}} \frac{\Delta\chi}{\chi} \frac{\dot{R}_\infty}{c_{sA}} \frac{R_0/R_c(1+R_0/R_c)}{R_0 + c_{sA}\,t}, \quad \omega_A(t) = -c_{sA}\,v_A(t). \tag{20}$$

The qualitative effect of the spin diffusion, neglected here, is the rounding of the magnetization step with $\omega\,t$ at the wave front. So Eq. (20) is valid for the total change in v_A and ω_A.

3 Growth Dynamics of spherical bubbles

The interface dynamics of superfluid ^{3}He is fundamentally different from other systems [7]. If $\dot{u} \ll c_2$, the evacuation of latent heat is very efficiently accomplished via second sound, the difference between hypercooling and normal supercooling is inessential, and $\dot{u}$ is determined by the Kapitza resistance of the interface. For $\dot{u} \gg c_2$, the system is always hypercooled, no heat evacuation needs to take place and not much does. $\dot{u}$ is determined by the growth coefficient.

In bubble growth, two similar scenarios prevail: For weak undercooling of the A-phase, $\dot{R} \ll c_2$, an outgoing radial wave is emitted into the A-phase, while an imploding wave is emitted into the bubble. The latter will interfere at the center of the bubble, as in the case of spin waves, yielding vanishing counterflow and an averaged temperature, depending only on the current bubble radius.

For strong undercooling, assuring $\dot{R} \gg c_2$ at all time, no sound is emitted into the A-phase, while an exploding and an imploding wave superpose inside the bubble, yielding a time dependent temperature distribution.

3.1 Bulk Hydrodynamics

We start from the linearized equations of bulk hydrodynamics (correct for both limits [7] $\dot{R} \gg c_2$, $\dot{R} \ll c_2$ but not in-between, $\dot{R} \approx c_2$ [13]), in a form appropriate for the spherical symmetry of the problem. As in planar growth, first sound is too fast to need

explicit consideration. Its only role is to maintain uniform pressure on both sides of the interface, while keeping the discontinuity $\Delta p = \alpha/R$ across it. This leaves two equations: Conservation of entropy and the equation for the counterflow. The counterflow, $\vec{w} = w(r)\,\hat{e}_r$ is curl-free and can be written as $w(r) = \partial_r \phi$. The two hydrodynamic equations then become

$$\frac{\rho\sigma}{\rho^n}\,\dot{\delta T} + c_2^2\,\Delta_r \phi = 0, \tag{21}$$

$$\partial_r \left(\dot{\phi} + \frac{\rho\sigma}{\rho^n}\,\delta T \right) = 0. \tag{22}$$

Eq. (22) seems to allow $\dot{\phi}$ and $-\rho\sigma/\rho^n\,\delta T$ differing by an explicit function of time. This is ruled out by the wave equation that can be obtained from the combination of (21) and (22), which must not have any time dependent source.

In summary, we end up with

$$w = \partial_r\,\phi(r,t), \quad \delta T = -\frac{\rho^n}{\rho\sigma}\dot{\phi}(r,t), \quad \ddot{\phi} - c_2^2 \Delta_r\,\phi = 0, \tag{23}$$

in close analogy to (11).

3.2 Weak undercooling

We will consider two different stages: The first stage is characterized by the existence of an incoming and an outgoing second sound wave and lasts only for a time span of order R_0/c_2, where $R_0 \equiv R(t=0)$. The second stage starts after the interference has established homogeneity inside the bubble, making the temperature solely dependent of the bubble radius. In the calculation of the second stage we shall neglect the existence of the first. This only changes the initial condition and hence the exact shape of the radial wave front but not its magnitude. For very weak undercooling, R_c is large compared to the quasiparticles mean free path, so that for $t = 0$ $R = R_c$ and $T = T_i$ are the valid initial conditions. Otherwise, we assume a nonvanishing initial temperature discontinuity $\Delta T_i = T_{iB} - T_{iA}$ and $R = R_0 \gg R_c$ at $t = 0$.

We expand the CoCos (3,5,7), to first order in $\dot{R}$, $\delta T_{A,B}$, $w_{A,B}$ around the initial temperature T_i:

$$
\begin{aligned}
0 &= -\rho\dot{R}\Delta\sigma_i + \rho^s\langle\sigma\rangle(w_B - w_A), && (24)\\
0 &= \Delta\mu_i(1+\frac{R_c}{R}) - \langle\sigma\rangle(\delta T_B + \Delta T_i - \delta T_A), && (25)\\
0 &= -\rho\dot{R}\langle\sigma\rangle - \kappa(\delta T_B + \Delta T_i - \delta T_A), && (26)
\end{aligned}
$$

all quantities refer to the laboratory frame. Terms of Order $(\Delta\sigma_i/\langle\sigma\rangle)^2$ as well as $\partial_p(\rho^s/\rho)$, $\partial_T(\rho^s/\rho)$ and $\Delta\rho/\rho$ are omitted.

From (25) and (26) we readily obtain the interface motion as quoted in Eq. (8). The limiting value of the interface velocity is

$$\dot{R}_\infty = -\frac{\kappa\,\Delta\mu_i}{\langle\sigma\rangle^2\,\rho}. \tag{27}$$

We consider the sound amplitudes at the interface for the first stage. Starting with

$$\phi(r,t) = \frac{f(r-c_2\,t)}{r} + \frac{g(r-c_2\,t)}{r},$$

we apply the method described in Sec. 2 and calculate the sound amplitudes to lowest order in $(R-R_c)/R_c$:

$$
\begin{aligned}
\delta T_{\substack{A\\B}} &= \mp\frac{\Delta\mu_i}{\langle\sigma\rangle} + \frac{1}{2}\Delta T_i - \frac{\dot{R}_\infty}{c_2}\frac{\Delta\sigma_i}{\langle\partial_T\sigma\rangle} && (28)\\
&\quad +\frac{1}{2}\left\{\frac{\Delta\mu_i}{\langle\sigma\rangle}\left(\frac{c_2}{\dot{R}_\infty}\pm 1\right) - \frac{1}{2}\Delta T_i\frac{c_2}{\dot{R}_\infty} - \frac{\dot{R}_\infty}{c_2}\frac{\Delta\sigma_i}{\langle\sigma\rangle}\right\}\frac{R-R_c}{R_c} + \mathcal{O}\left(\left(\frac{R-R_c}{R_c}\right)^2\right),\\
w_{\substack{A\\B}} &= \frac{\rho\langle\sigma\rangle}{\rho^n c_2}\left[-\frac{\Delta\mu_i}{\langle\sigma\rangle} + \frac{1}{2}\Delta T_i \mp \frac{\dot{R}_\infty}{c_2}\frac{\Delta\sigma_i}{\langle\partial_T\sigma\rangle}\right. && (29)\\
&\quad +\frac{1}{2}\left\{\frac{\Delta\mu_i}{\langle\sigma\rangle}\left(\pm 2\frac{c_2}{\dot{R}_\infty}+3\right) - \Delta T_i\left(\pm\frac{c_2}{\dot{R}_\infty}+1\right) - \frac{\Delta\sigma_i}{\langle\partial_T\sigma\rangle}\left(1\pm 3\frac{\dot{R}_\infty}{c_2}\right)\right\}\frac{R-R_c}{R_c}\\
&\quad \left.+\mathcal{O}\left(\left(\frac{R-R_c}{R_c}\right)^2\right)\right].
\end{aligned}
$$

Setting ΔT_i and $R-R_c$ to zero, these expressions can be compared to the results of planar growth [7]: As it turns out, the surface tension doubles the initially emitted sound amplitudes. Note that the terms of first order in R/R_c-1 are dominated by the contribution proportional to $c_2/\dot{R}_\infty$.

For the second stage, the situation is quite similar to that of spinwaves, examined in the last section. Since (25) and (26) have already been used once to determine the bubble radius as a function of time, we shall now only consider the CoCos (24) and (25). With w_B vanishing, (24) simplifies to

$$0 = \rho\,\Delta\sigma_i\,\dot{R} + \rho^s\langle\sigma\rangle\,w_A, \tag{30}$$

which is analog to (13) when w_A is identified with $-v_A$. Combining (30) with (25) yields

$$w_A = \frac{\kappa\,\Delta\sigma_i}{\langle\sigma\rangle^2\,\rho^s}\left(\delta T_B - \delta T_A + \Delta T_i\right). \tag{31}$$

By identification of δT_A with ω_A, (31) is analogous to (12). (These identifications are justified by inspection of the bulk hydrodynamics: (23) goes over into (11) by the substitution of $-\Theta_A$ for ϕ; but this does not alter the solution of the wave equation.)

We can therefore take over the results of Sec. 2 by setting

$$w_A = -v_A, \tag{32}$$

$$\delta T_A = \frac{\rho^n}{\rho\langle\sigma\rangle}\frac{c_{2A}}{c_{\mathrm{s}A}}\omega_A, \tag{33}$$

when we in addition observe the respective redefinition of A and c_A,

$$A = -\frac{\Delta\sigma_i}{\langle\sigma\rangle}\frac{\rho^s}{\rho}\dot{R}_\infty\,R_c, \quad c_A = \frac{c_{2A}}{\dot{R}_\infty}, \tag{34}$$

introduced in App. B. As a consequence of this analogy, Figs. 2 and 3 also serve as illustrations of counterflow and temperature amplitudes.

3.3 Strong undercooling

At the strong degree of undercooling we are considering here, the hydrodynamic description only holds after the bubble has grown to an appropriate multiple of the critical size. We therefore impose the initial condition $R(t=0) = x_0\,R_c$ with $x_0 \gg 1$.

Inside the bubble, an incoming and an outgoing second sound wave superpose. After the incoming wave front has been "reflected" at the center of the bubble, there are two

spherical discontinuities of temperature and counterflow, expanding outward and laging behind the third discontinuity, at the bubble surface.

Neglecting terms of the order $w_B/\dot{R}$, an expansion of (3,5,7), again in $R_c/R-1$, yields for the discontinuities at the bubble surface

$$0 = T_i\Delta\sigma_i + \Delta\mu_i\left(1+\frac{R_c}{R}\right) + T_i\,\partial_T\sigma_B\,\left(\delta T_B + \Delta T_i\right), \tag{35}$$

$$0 = \Delta\mu_i\left(1+\frac{R_c}{R}\right) - \sigma_B\left(\delta T_B + \Delta T_i\right) + \frac{\rho^n}{\rho}\dot{R}\,w_B, \tag{36}$$

$$\frac{\rho\dot{R}}{K} = T_i\Delta\sigma_i + \left(T_i\partial_T\sigma_B + \frac{\Delta\sigma_i}{2}\right)\left(\delta T_B + \Delta T_i\right). \tag{37}$$

From (35) we obtain the temperature

$$\delta T_B = -\Delta T_i - \frac{\Delta\mu_i}{T_i\partial_T\sigma_B}\left(\frac{1+R/R_c}{R/R_c}\right) - \frac{\Delta\sigma_i}{\partial_T\sigma_B}, \tag{38}$$

which, together with (37), again leads to (8). Here the limiting value of the interface velocity is

$$\dot{R}_\infty = -\frac{K\Delta\mu_i}{\rho}\left(1+\frac{1}{2}\frac{\Delta\sigma_i}{T_i\partial_T\sigma_B}\right). \tag{39}$$

By calculation of the total counterflow amplitude

$$w_B = -\frac{\rho}{\rho^n}\left\{\frac{\Delta\mu_i}{\dot{R}_\infty}\left(1+\frac{\sigma_B}{T_i\partial_T\sigma_B}\right) + \frac{\sigma_B\Delta\sigma_i}{\partial_T\sigma_B}\frac{1}{\dot{R}}\right\}, \tag{40}$$

our initial neglect of $\mathcal{O}(w_B/\dot{R})$ proves to be appropriate.

4 Interacting Bubbles

As mentioned in the introduction, we expect the growth velocity of the bubble to slow down, when its surrounding heats up from second sound radiation sent out by other bubbles. Only the case of weak undercooling ($\dot{R} < c_2$) is worth studying, since for strong undercooling ($\dot{R} > c_2$) all the latent heat remains inside the bubble.

Let us for simplicity consider a volume V of A-phase, containing N B-phase bubbles, nucleated simultaneously and distributed uniformly over V. Each individual bubble grows as described in the preceding section until it is reached by the second sound pulses of its

neighbors. From now on, the accumulative heating of the A-phase increasingly hinders the evacuation of latent heat and slows down the growth velocity.

We will restrict our calculations to the regime where the temperatures of both the A- and B-phase can be regarded as being uniform. The Volume V is thus divided up into two subsystems: N bubbles of total volume $V_o = N4\pi/3R^3$ and the remaining A-phase of volume $V - V_o$. Since the gradients vanish, the local hydrodynamic description of the previous sections reduce to thermodynamic considerations: For small deviations from equilibrium, energy conservation accounts for equality of the entropy currents,

$$\dot{S}_B = -\dot{S}_A, \tag{41}$$

where $S_B = V_o\,\rho\,\sigma_B$ and $S_A = (V - V_o)\,\rho\,\sigma_A$ denote the total entropies of the respective phase. Because of the identity

$$d_t\,S_B = \int_{V_o} dV\,\dot{\sigma}_B + \int_{\partial V_o} ds\,\dot{R}\sigma_B = -\int_{\partial V_o} ds\,f'_B, \tag{42}$$

we identify Eq. (41) as the continuity condition of the local entropy current, integrated over the area of the interface. In the same manner, we obtain the Onsager relation, starting from $f'_B = \kappa\,\Delta T$ as

$$-\frac{\dot{S}_B}{A_I} = \kappa\,(\delta T_B - \delta T_A). \tag{43}$$

Here, A_I denotes the area of the interface so that the total rate of interface entropy production is an extensive function with respect to the interface area, as it must be. Being of intensive nature, the continuity condition for the phase angle

$$0 = \Delta\mu_i\left(1 + \frac{R_c}{R}\right) - \sigma_B\,\delta T_B + \sigma_A\,\delta T_A \tag{44}$$

does not change its appearance.

Because of the homogeneity of the subsystems, all thermodynamic quantities are explicit functions of R. We therefore need to specify only a single initial condition:

$$\delta T_B(R_i) - \delta T_A(R_i) = \Delta\,T_i, \tag{45}$$

where R_i denotes the initial bubble radius and ΔT_i is the temperature difference that was built up across the interface during the switch-on process. From Sec. 3, we expect ΔT_i to be of the order $\Delta\mu_i/\langle\sigma\rangle$. Since (44) was already valid before homogeneity had been established, the initial temperature amplitudes are found to be

$$\delta T_A(R_i) = \frac{\Delta\mu_i - \sigma_B\,\Delta T_i}{\Delta\sigma_i}, \quad \delta T_B(R_i) = \frac{\Delta\mu_i - \sigma_A\,\Delta T_i}{\Delta\sigma_i}. \tag{46}$$

Here and below, we neglect the effect of interface tension, i.e. we assume $R_c \ll R_i$.

From (41) and the derivative of (44) with respect to R we obtain $\partial_R\delta T_A$ and $\partial_R\delta T_B$ which may be integrated to give the temperature amplitudes as functions of the bubble radius:

$$\delta T_{A,B}(R) = \delta T_{A,B}\,(R_i) - \frac{\sigma_{B,A}\,\Delta\sigma_i}{a}\,\ln\left(\frac{4\pi/3NR^3\,a + V\,b}{4\pi/3NR_i^3\,a + V\,b}\right), \tag{47}$$

with $a = \sigma_A\,\partial_T\sigma_B - \sigma_B\,\partial_T\sigma_A$, $b = \sigma_B\,\partial_T\sigma_A$.

The growth velocity follows from (43):

$$\dot{R}(R) = -\frac{\kappa}{\rho}\Delta T_i\frac{\delta T_B(R) - \delta T_A(R)}{\sigma_B + \partial_T\sigma_B\,R\,\partial_R\delta T_B/3}. \tag{48}$$

Obviously, the system approaches an equilibrium state with equal temperatures on both sides of the interface and vanishing $\dot{R}$. Starting with

$$\dot{R}(R_i) \approx -\frac{\kappa}{\rho}\frac{\Delta T_i}{\langle\sigma\rangle}\left(1 - \frac{\Delta\sigma_i}{\langle\sigma\rangle}\left\{\frac{1}{2} - \frac{4\pi/3NR_i^3}{V}\right\}\right),$$

the interface velocity decreases and eventually comes to rest at the final bubble radius R_f. The B-phase bubbles then occupy the volume

$$\frac{4\pi}{3}NR_f^3 = \frac{1}{a}\left\{\left(\frac{4\pi}{3}NR_i^3\,a + V\,b\right)\exp\left(-\frac{a\,\Delta T_i}{\Delta\sigma_i^2}\right) - V\,b\right\} \tag{49}$$

and the final temperature amplitudes amount to

$$\delta T_A(R_f) = \delta T_B(R_f) = \frac{\Delta\mu_i}{\Delta\sigma_i}. \tag{50}$$

A Calculation of $x(\tau)$

For convenience, we introduce reduced dimensionless variables by $x = R/R_c$ and $\tau = t/t_c$, where $t_c = R_c/\dot{R}_\infty$ is the characteristic time for interface movement. The solution (9) of the equation of motion of the bubble radius (8) then takes the form

$$\tau(x) = x - x_0 + \ln\left(\frac{1+x_0}{1+x}\right), \tag{51}$$

which shall now be inverted to yield the bubble radius as a function of time.

The inverse of $z \mapsto z\,e^z$, is known as Lambert's function W [14]. For real valued x, W has two branches:

$$\begin{aligned} W_0(x) \geq -1 \quad &; \quad -\frac{1}{e} \leq x \\ W_{-1}(x) \leq -1 \quad &; \quad -\frac{1}{e} \leq x \leq 0 \end{aligned}$$

Exponentiation of (51) yields

$$-(1+x)e^{-(1+x)} = -(1+x_0)e^{-(1+x_0)}e^{-\tau}.$$

By definition of W this is equivalent to

$$x(\tau) = -1 - W_{-1}\left(-(1+x_0)e^{-(1+x_0)}e^{-\tau}\right)$$

W_{-1} is the right branch, because the argument is always negative, and x must not be limited.

Note that we reserve x and τ to denote the reduced bubble radius and the corresponding reduced time, respectively. Arbitrary coordinates (r,t) are referred to by (y,ϑ), see App. B.

B Spin wave amplitudes

With $y = r/R_c$, $\vartheta = t/t_c$, $\varphi(y,\vartheta) = \Theta_A(r,t)$, $\bar{v}_A = v_A R_c$, $\bar{\omega}_A = \omega_A\, R_c/c_{\mathrm{s}A}$, $c_A = c_{\mathrm{s}A}/\dot{R}_\infty$, Eqs. (11) read

$$\bar{v}_A = \partial_y\,\varphi, \quad \bar{\omega}_A = \partial_\vartheta\,\varphi, \quad \partial_\vartheta^2\varphi - c_A^2\Delta_y\,\varphi = 0, \tag{52}$$

while the CoCos (12) and (13) become

$$0 = \Delta\bar{\omega}, \quad 0 = A\,\partial_\tau x + \bar{v}_A, \quad \text{with} \quad A = -\frac{\Delta\chi}{\chi_A}\frac{\gamma H}{c_{\mathrm{s}A}^2}\dot{R}_\infty\, R_c > 0. \tag{53}$$

The general solution of (52) is $\varphi(y,\vartheta) = F(y - c_A\,\vartheta)/y$. Inserting $\bar{v}_A\,|_I = F'\,|_I\,/x - F\,|_I\,/x^2$ and $\bar{\omega}_A\,|_I = -F'\,|_I\,/x$, with

$$F\,|_I = F(x - c_A\tau(x)) = q(x), \quad F'\,|_I = \frac{\partial_x q(x)}{1 - c_A\partial_\tau x}, \tag{54}$$

into the CoCos (53), we obtain the following differential equation for $q(x)$:

$$\partial_x q(x) = \frac{x(1-c_A)+1}{x(1+x)}q(x) - A\,(x\,(1-c_A)+1)\,. \tag{55}$$

The special solution of (55) subject to the initial condition $q(x_0) = 0$ is

$$\begin{aligned} q(x) &= -A\frac{x}{(1+x)^{c_A}}\,(C(x) - C(x_0)) \quad \text{with} \\ C(x) &= \frac{1-c_A}{1+c_A}(1+x)^{1+c_A} + \frac{1}{c_A}(1+x)^{c_A}\,{}_2\mathrm{F}_1(-c_A, 1; -c_A+1; \frac{1}{1+x}). \end{aligned} \tag{56}$$

Here, ${}_2F_1$ denotes the hypergeometric function as defined in [15], Eq. (7-76). Choosing $x_1(y,\vartheta)$ so that,

$$F\,(x_1(y,\vartheta) - c_A\,\tau\,(x_1(y,\vartheta))) = F(y - c_A\,\vartheta), \tag{57}$$

we obtain the spin wave amplitudes outside the bubble as

$$\bar{v}_A(y,\vartheta) = \frac{1}{y}\,\frac{\partial_x q(x)}{1 - c_A\,\partial_x\tau(x)}\bigg|_{x=x_1(y,\vartheta)} - \frac{1}{y^2}q(x)\,|_{x=x_1(y,\vartheta)} \tag{58}$$

$$\bar{\omega}_A(y,\vartheta) = -\frac{1}{y}\,\frac{\partial_x q(x)}{1 - c_A\,\partial_x\tau(x)}\bigg|_{x=x_1(y,\vartheta)}. \tag{59}$$

A closed form expression for $x_1(y,\vartheta)$ is derived in App. C.

C Calculation of $x_1(y,\vartheta)$

A necessary condition for (57) to be fulfilled is given by

$$x_1 - c_A\,\tau(x_1) = y - c_A\,\vartheta.$$

Inserting the definition (9) of $\tau(x)$ gives after exponentiation

$$\frac{1-c_A}{c_A}(1+x_1)\,e^{\frac{1-c_A}{c_A}(1+x_1)} = \frac{1-c_A}{c_A}(1+x_0)\,e^{\frac{1-c_A}{c_A}}\,e^{-x_0}\,e^{\frac{y-c_A\,\vartheta}{c_A}},$$

so that

$$x_1(y,\vartheta) = -1 + \frac{c_A}{1-c_A}W_{-1}\left(\frac{1-c_A}{c_A}(1+x_0)\,e^{\frac{1-c_A}{c_A}}\,e^{-x_0}\,e^{\frac{y-c_A\,\vartheta}{c_A}}\right).$$

To check for the right branch, we make use of the identity

$$\begin{aligned} x &= x_1(x,\tau(x)) \\ &= -1 + \frac{c_A}{1-c_A}W_{-1}\left(\frac{1-c_A}{c_A}(1+x)\,e^{\frac{1-c_A}{c_A}(1+x)}\right). \end{aligned}$$

Since $c_A > 1$, the argument of W_{-1} is negative. W_{-1} is the right branch, because x has to be a monotonic function of itself.

References

[1] D. S. Buchanan, G. W. Swift and J. C. Wheatley, *Phys. Rev. Lett.*, **57**, 341 (1986).

[2] S. T. P. Boyd and G. W Swift, *Phys. Rev. Lett.*,**64**, 894, (1990).

[3] S. T. P. Boyd and G. W Swift, *J. Low. Temp. Phys.*, **87**, 35, (1992).

[4] S. T. P. Boyd and G. W Swift, *J. Low. Temp. Phys.*, **86**, 325, (1992).

[5] S. Yip and A. J. Leggett, *Phys. Rev. Lett.*, **57**, 345 (1986); A. J. Leggett and S. K. Yip, in *Helium Three*, W. P. Halperin and L. P. Pitaevskii, eds. (Elsevier, Amsterdam 1990); A. J. Leggett, *J. Low. Temp. Phys.*, **87**, 571, (1992).

[6] J. Palmeri, *Phys. Rev. Lett.*, **62**, 1872 (1989); N. B. Kopnin, *Zh. Eksp. Theor. Fiz.*, **92**, 2106, (1987) [*Sov. Phys. JETP*, **65**, 1187, (1987)].

[7] M. Grabinski and M. Liu, *Phys. Rev. Lett.*, **65**, 2666 (1990).

[8] P. Panzer and M. Liu, *Phys. Rev. Lett.*, **69**, 3658, (1992). *J. Low. Temp. Phys.*, to be published in June 1993

[9] P. Kostädt and M. Liu, *to be published.*

[10] D. Vollhardt and P. Wölfle, *The Superfluid Phases of Helium 3*, Taylor and Francis, London (1990), sec. 10.2 and sec. 7.2.

[11] We have put $\alpha = -2\sigma_{AB}$. σ_{AB} is the interfacial energy as introduced in D. D. Osheroff and M. C. Cross, *Phys. Rev. Lett.*, **38**, 905, (1977); R. Kaul and H. Kleinert, *J. Low. Temp. Phys.*, **38**, 539, (1980); N. Schopohl, *Phys. Rev. Lett.*, **58**, 1664, (1987).

[12] E. V. Thuneberg, *Physica B* **178**, 168 (1992).

[13] J. Johannesson and M. Liu *to be published.*

[14] R. M. Corless, G. H. Gonnet, D. E. G. Hare, and D. J. Jeffrey, *technical report CS-93-03*, Universtiy of Waterloo, Canada, (1993). Also available via anonymous ftp from `cs-archive.uwaterloo.ca` as `cs-archive/CS-93-03/W.ps.Z`.

[15] J. Mathews and R. L. Walker, *Mathematical Methods of Physics*, Addison-Wesley, (1970).

Figure Captions

Figure 1: Mean free path l_{QP} of quasi particles in the B-phase (taken from Fig. 10.1 of Ref. [10]) and critical bubble radius R_c (as given by Kaul and Kleinert [11]),both as functions of temperature.

Figure 2: Counterflow and spin-superfluid velocity, scaled as $w_A \left(-\frac{\Delta\sigma_i}{\langle\sigma\rangle}\frac{\rho^s}{\rho}\dot{R}_\infty\right)^{-1} = -v_A \left(-\frac{\Delta\chi}{\chi_A}\frac{\gamma H}{{c_s}_A^2}\dot{R}_\infty\right)^{-1}$.

Figure 3: Temperature and excess magnetization, scaled as $\delta T_A \frac{\rho\langle\sigma\rangle}{\rho^n c_{2A}} \left(-\frac{\Delta\sigma_i}{\langle\sigma\rangle}\frac{\rho^s}{\rho}\dot{R}_\infty\right)^{-1} = \frac{\omega_A}{{c_s}_A} \left(-\frac{\Delta\chi}{\chi_A}\frac{\gamma H}{{c_s}_A^2}\dot{R}_\infty\right)^{-1}$.

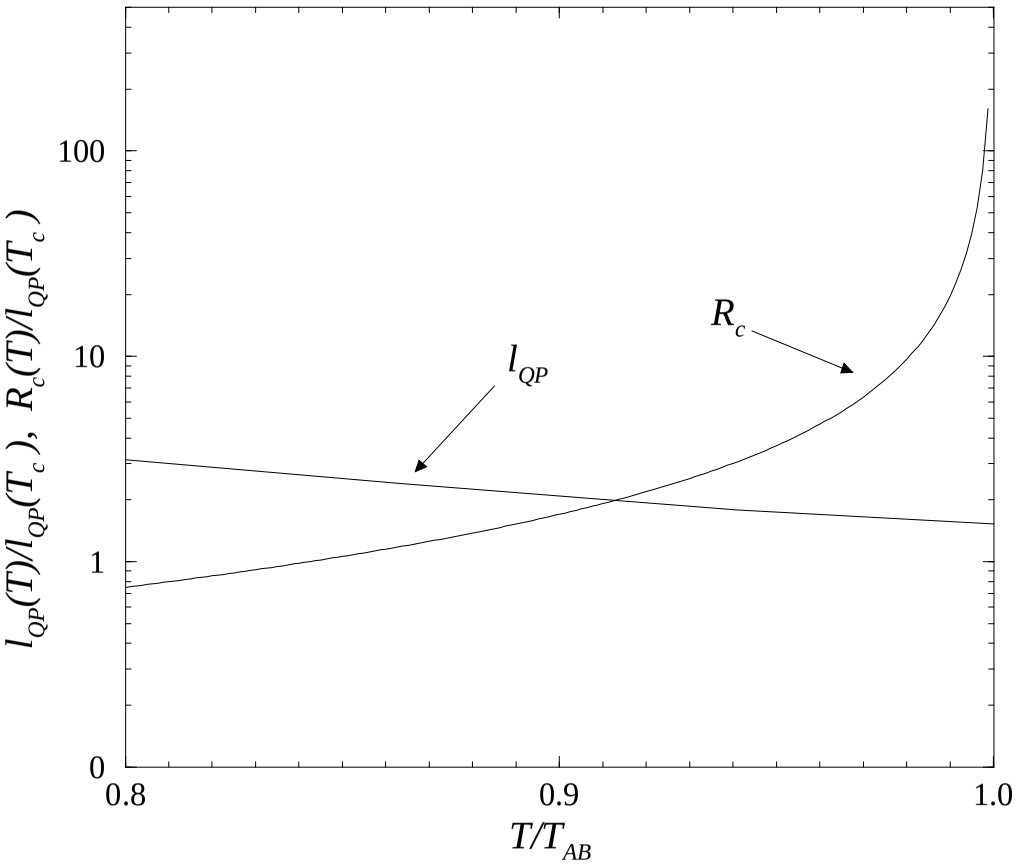

Figure 1

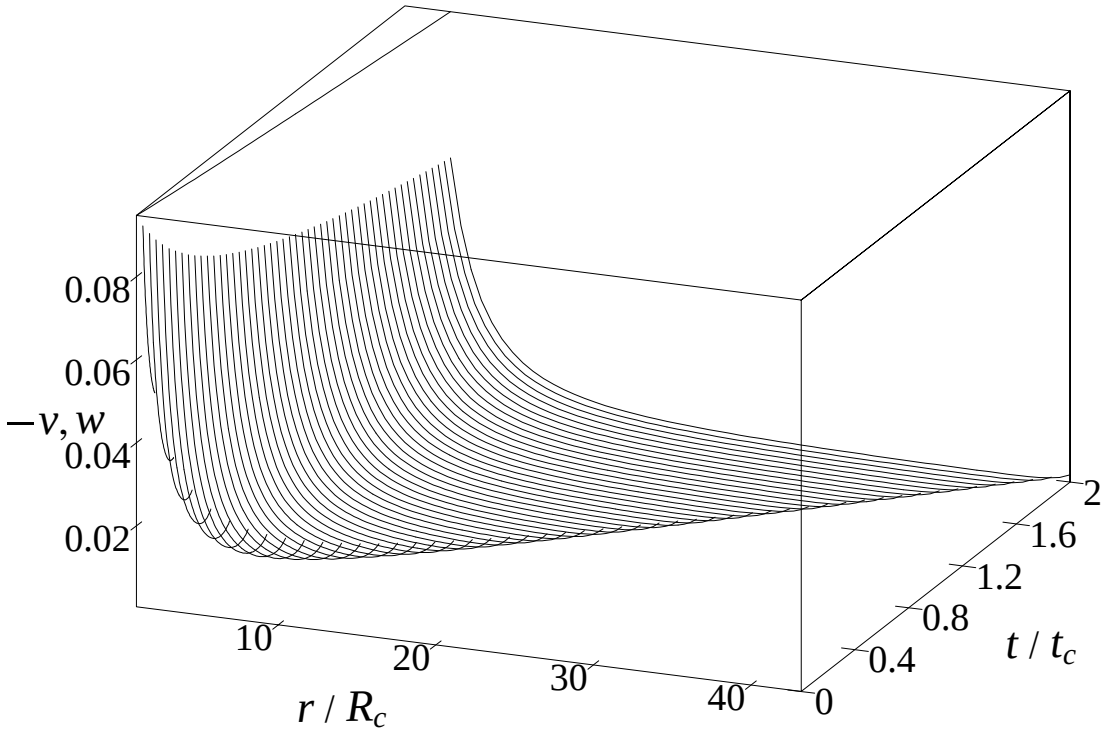

Figure 2

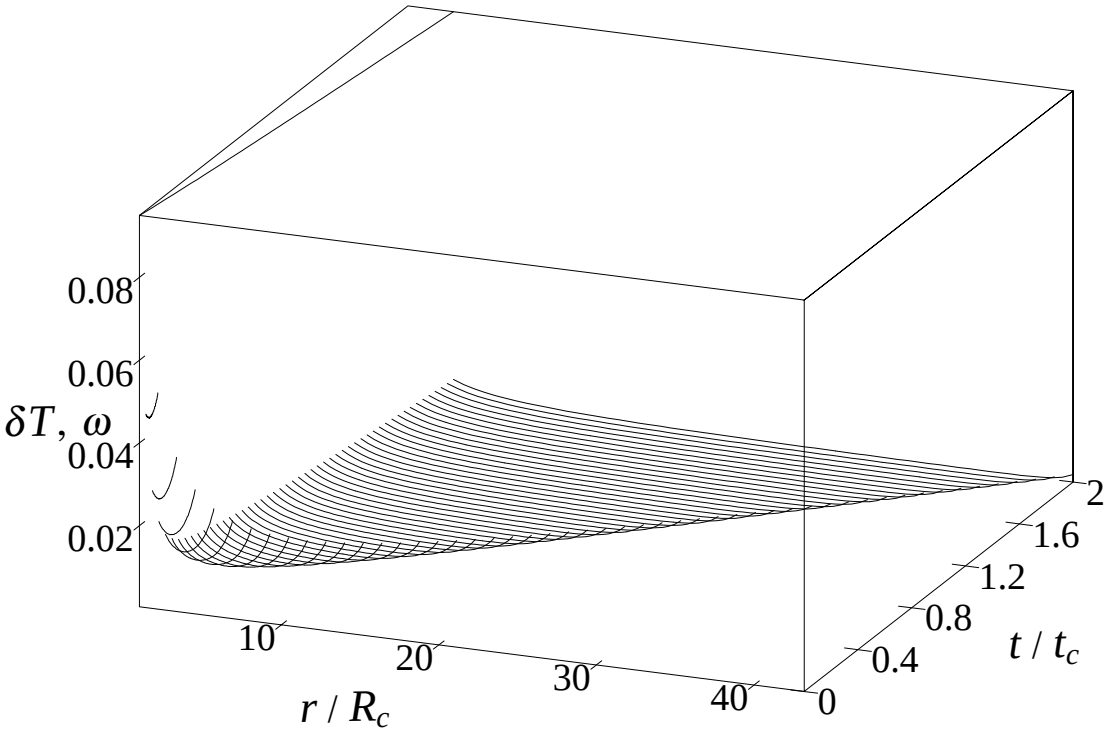

Figure 3